Supporting Information

Buhrman et al. 10.1073/pnas.0912226107

SI Text

Hydrogen Bonding Network Involving Q61 and Y32 in the Ordered Active Site. In addition to interacting with the side chain of E62 through W176, the side chain of Q61 H-bonds to the active site water molecule, W189, through its other lone pair electrons. Water molecule W176 also links Q61 to the side chain of R68 as well as to helix 3 residues D92 and Y96 through an H-bonding network involving W9, W28, and W367 (Fig. S1). While the side chain of Q61 is involved in this network, its carbonyl group is bridged to the side chain of R68 through water molecule W372.

Due to resonance stabilization involving the aromatic ring, the Y32 hydroxyl oxygen atom has its two lone pairs confined to the plane of the ring. Thus, in addition to its interaction with the active site bridging water molecule W189, it is involved in an H-bonding network through which it is linked to the side chain of N86 at the beginning of helix 3. The C-terminal end of helix 3 is at the center of the allosteric switch. This network is shown in detail in Fig. S1.

Structure of RasY32F-GppNHp. Fig. S2 shows two of the three molecules in the asymmetric unit found in the structure of RasY32F-GppNHp. In one of the monomers, shown in blue in Fig. S2, both active site water molecules are present. They appear to be due to the correct placement of T35, which in the other two monomers is flipped out of the active site. The third molecule in the asymmetric unit does not overlap either of the other two, but has similar characteristics to the monomer shown in maroon with respect to its relationship to the active site.

Raf Binds to RasY32F-GppNHp but not to RasY32F-GDP. In order to determine whether Raf binds to the RasY32F mutant in a nucleotide-dependent manner, we used Raf-RBD-CRD, a construct of Raf that includes both the RBD and CRD Ras-binding domains. This construct, containing residues 52–184 of Raf fused at the N terminus to a 56-residue immunoglobulin-binding domain of streptococcal protein G (GB1 domain) (1) was used for all experiments involving Raf. GB1-Raf-RBD-CRD (52–184) was cloned into the pET21a vector (Novagen) using Nde1 and EcoRI restriction sites (NE Biolabs). The fusion protein increases protein expression and solubility, and we have shown previously that it does not interfere with binding wild-type Ras (2). The plasmid was transformed into BL21 cells for protein expression. Cells were grown in LB in the presence of ampicillin and induced with 1.0 mM IPTG in the presence of 200 μM $ZnCl_2$. Pellets were stored at −80 °C. Pellets were resuspended in 20 mM Hepes (pH 7.0), lysed, and the protein was purified using cation exchange chromatography in a HiLoad 26/10 SP sepharose column (Amersham Pharmacia). The Raf-containing fractions were concentrated to less than 10 mL and further purified using a HiPrep 26/60 S200 gel filtration column (50 mM Tris, pH 7.0). GB1-Raf-RBD-CRD was concentrated to 2–5 mg/mL and stored as frozen aliquots at −80 °C.

For the binding experiments Raf-RBD-CRD was incubated in a 1:1 molar ratio with either RasY32F-GppNHp or RasY32F-GDP at a concentration of 10 μM and analyzed by gel filtration chromatography. Each protein solution was in a total of 2 mL buffer consisting of 50 mM Tris pH 7.5, 1 mM DTT, 50 mM NaCl, and 1 mM $MgCl_2$. After 30 min, the samples were run on a cold S-100 column, preequilibrated in the buffer solution plus 10% glycerol. Fig. S3*A* shows the elution profile for the RasY32F-GppNHp/Raf-RBD-CRD, and Fig. S3*B* shows RasY32F-GDP/Raf-RBD-CRD solutions superimposed on the elution profile of a solution containing a 2:1 molar ratio of wild-type Ras-GppNHp and Raf-RBD-CRD. The Ras/Raf complex elutes as a peak at 52 mL, while free Ras and free Raf-RBD-CRD both elute at 62 mL. Both wild-type Ras-GppNHp and RasY32F-GppNHp form complexes with Raf, whereas their GDP-bound forms do not (Fig. S3).

Hydrolysis Experiments for Ras and RasY32F in the Absence and Presence of Raf-RBD-CRD. Ras protein was purified bound to GDP as described in *Materials and Methods*. The bound GDP was exchanged for γ^{32}P labeled GTP, following an exchange protocol adapted from Self and Hall (3). Ras-GDP (5 μg) was incubated at 30 °C for 15–20 min with 2 μCi of γ^{32}P GTP in an exchange buffer consisting of 50 mM Tris pH 7.5, 5 mM DTT, 50 mM NaCl, and 10 mM EDTA in a total volume of 50 μL. Immediately after the incubation, the exchange reaction was chilled on ice. $MgCl_2$ was then added to a concentration of 1 mM, and the solution passed over a cold P-6 nucleotide-binding column preequilibrated in a hydrolysis buffer (50 mM Tris pH 7.5, 1 mM DTT, 50 mM NaCl). In control experiments with equivalent amounts of Raf (which does not bind GTP), radioactivity that passed through the desalting column was approximately 5% of the radioactivity in similar GTP-labeled Ras samples and was lower than background subtracted counts. Therefore, radioactivity that passes through the nucleotide-binding column is specifically bound to Ras, and the measured hydrolysis rate approximates single turnover conditions.

Rates of intrinsic hydrolysis for wild-type Ras and RasY32F were obtained using γ^{32}P labeled GTP as previously published (4–6). In short, 2.5–3 μg of Ras-GTPγ^{32}P (or RasY32F-GTPγ^{32}P) was incubated at 30 °C with or without a stoichiometric amount of Raf-RBD-CRD in a total volume of 200–300 μL, for a final concentration of approximately 400 nM RasGTP/Raf-RBD-CRD complex. At multiple time points, 25 μL aliquots were removed from the reaction and the hydrolysis reaction quenched with 400 μL of a precooled solution consisting of 5% activated charcoal, 0.2 M HCl, 1 mM NaH2PO4, and 20% EtOH. This causes the nucleotide-bound protein to precipitate and adsorb to the charcoal. The samples are then centrifuged at 10,000 rpm for 10 min in a tabletop centrifuge, leaving the supernatant containing ^{32}P labeled inorganic phosphate of the hydrolysis reaction. Next, 200 μL of the supernatant solutions were added to scintillation vials containing 1.2 mL of liquid scintillation cocktail (ScintiVerse II from Fisher Scientific) and the $^{32}P_i$ quantified by scintillation counting. The counts were converted to % hydrolysis by the formula: (count − initial count)/(final count − initial count)*100. Fig. S4 shows the resulting plots of percent of hydrolysis vs. time fit to the equation $y = A^* \exp[-(x - x_0)/t_0] + C$ in Kaleidograph, following a method described by Shutes and Der (6).

Data Collection and Structure Refinement. Data collection and refinement statistics are presented in Table S1 for the five structures discussed in this article. Synchrotron data were collected at 100 K for wild-type Ras-GppNHp crystals grown in the presence of calcium acetate taken directly from the mother liquor and for the RasY32F-GppNHp mutant. The three datasets from crystals soaked in $Ca(OAc)_2$, $Mg(OAc)_2$, or backsoaked from $Mg(OAc)_2$ to $Ca(OAc)_2$ were collected at our home institution at 120 K on a MAR345 area detector mounted on a Rigaku RuH3R generator operating at 50 kV and 100 mA.

Data were processed using Denzo HKL or HKL2000 (7) and refined with *PHENIX* (8) and Coot (9).

1. Huth JR, *et al.* (1997) Design of an expression system for detecting folded protein domains and mapping macromolecular interactions by NMR. *Protein Sci* 6(11): 2359–2364.
2. Buhrman G, Wink G, Mattos C (2007) Transformation efficiency of RasQ61 mutants linked to structural features of the switch regions in the presence of Raf. *Structure* 15(12):1618–1629.
3. Self AJ, Hall A (1995) Measurement of intrinsic nucleotide exchange and GTP hydrolysis rates. *Methods Enzymol* 256:67–76.
4. Holden JL, *et al.* (1991) Rsr1 and Rap1 GTPases are activated by the same GTPase-activating protein and require threonine 65 for their activation. *J Biol Chem* 266(26): 16992–16995.
5. Leupold CM, Goody RS, Wittinghofer A (1983) Stereochemistry of the elongation factor Tu X GTP complex. *Eur J Biochem* 135(2):237–241.
6. Shutes A, Der CJ (2005) Real-time in vitro measurement of GTP hydrolysis. *Methods* 37(2):183–189.
7. Otwinowski Z, Minor W (1997) Processing of x-ray diffraction data collected in oscillation mode. *Methods in Enzymology,* Macromolecular Crystallography, Part A, eds Carter CW & Sweet RM (Academic Press, New York), Vol 276, pp 307–326.
8. Adams PD, *et al.* (2002) *PHENIX*: Building new software for automated crystallographic structure determination. *Acta Crystallogr, Sect D: Biol Crystallogr* D58:1948–1954.
9. Emsley P, Cowtan K (2004) Coot: Model-building tools for molecular graphics. *Acta Crystallogr, Sect D: Biol Crystallogr* D60:2126–2132.

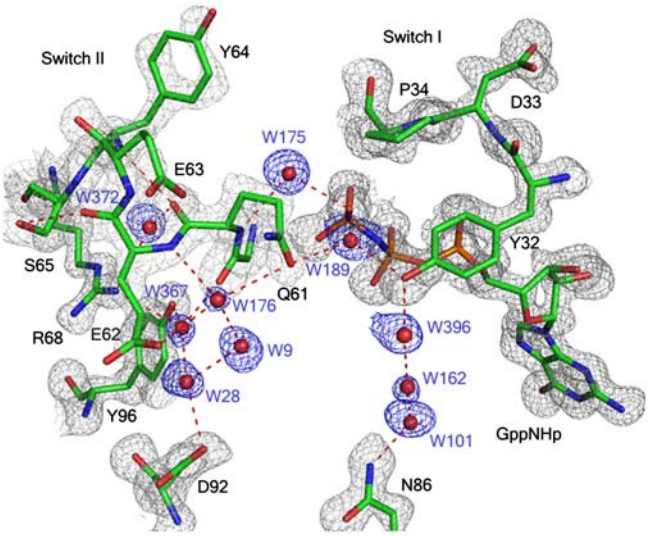

Fig. S1. Switch I and switch II in the well-ordered active site in Ras-GppNHp. The 2Fo-Fc electron density map drawn around protein atoms and the nucleotide is contoured at the 1σ level and depicted in gray. The map showing the network of water molecules connecting switch II and the active site with helix 3 is contoured at the 1.3σ level and depicted in blue for clarity. The residue numbers are given in the corresponding color scheme.

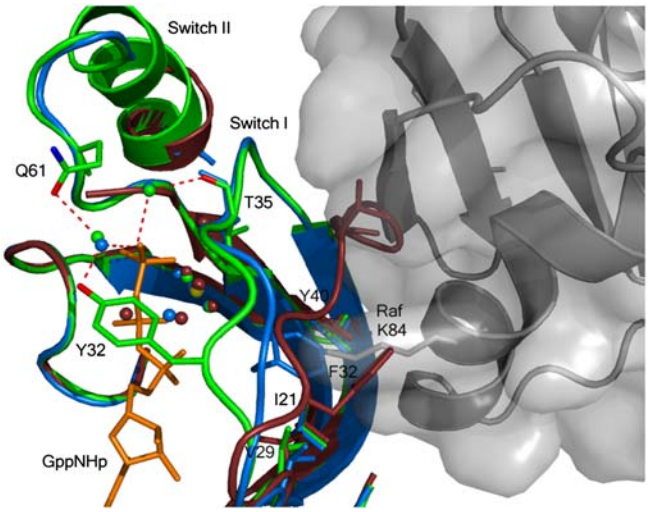

Fig. S2. Switch regions in RasY32F-GppNHp. Wild-type Ras-GppNHp with ordered switch II is shown in green with hydrogen bonds involving the catalytic and bridging water molecules depicted in red dashed lines. Two of the three models in the asymmetric unit of the mutant, superimposed on the wild type by least squares fit of the nucleotide atoms, are colored as follows: Chain A is in blue and Chain C is in maroon. Chain B is omitted for clarity, but it also occludes the Raf-RBD binding pocket. Water molecules are shown as spheres and color-coded according to their corresponding protein models. The Raps/Raf-RBD complex (from PDB code 1GUA) was superimposed on our wild-type Ras-GppNHp structure, and the Raf-RBD model (without Raps) is depicted in gray to show its binding site on Ras.

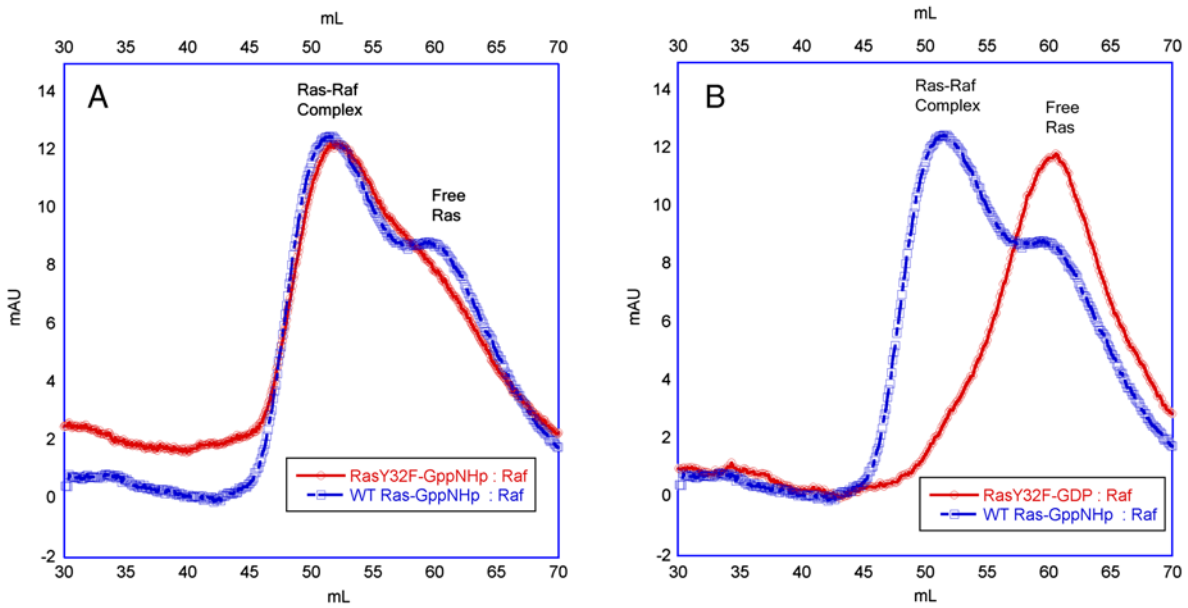

Fig. S3. Chromatogram of RasY32F-GppNHp and RasY32F-GDP in the presence of Raf-RBD-CRD resulting from gel filtration through a S-100 column. In both panels *A* and *B* the elution profile of a 2:1 molar ratio of wild-type Ras-GppNHp:Raf-RBD-CRD is shown in blue. The first peak centered at 52 mL corresponds to the complex, and the second peak centered at 62 mL corresponds to the excess free Ras-GppNHp. (*A*) A 1:1 molar ratio of RasY32F-GppNHp:Raf-RBD-CRD elutes primarily at 52 mL as shown in red. This peak coincides with that for the wild-type complex and supports formation of the mutant complex. (*B*) A 1:1 molar ratio of RasY32F-GDP:Raf-RBD-CRD is shown in red to elute at 62 mL where free Ras elutes. This peak contains a mixture of free Ras-GDP (19 kDa) and free Raf-RBD-CRD (22 kDa), which elute together in the S-100 column.

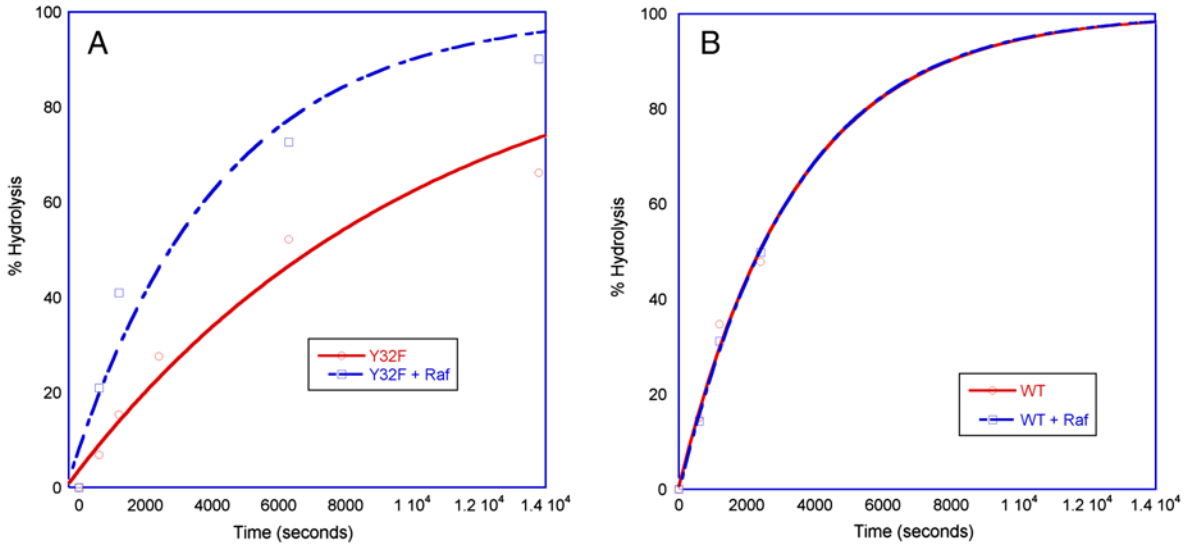

Fig. S4. Plots of percent hydrolysis vs. time in the conversion of GTP to GDP + P_i catalyzed by either wild-type Ras or RasY32F. Turnover rates are derived from fitting the data to the equation $y = ml^* \exp[-(x - m2)/m3] + 100$, where $m2 = x_0$ and $m3 = t_0$. (*A*) Hydrolysis curves for RasY32F in the absence (red) and presence (blue) of Raf-RBD-CRD yield turnover rates of 0.006 + / − 0.001 min^{-1} and 0.014 + / − 0.001 min^{-1} respectively. (*B*) Hydrolysis curves for wild-type Ras in the absence (red) and presence (blue) of Raf-RBD-CRD both yield a turnover rate of 0.016 + / − 0.002 min^{-1}. The hydrolysis rates are averages from at least two independent experiments.

Table S1.

	WT Ras	Ca acetate soak	Mg acetate soak	Ca acetate backsoak	RasY32F
Space group	R32	R32	R32	R32	P2(1)2(1)2(1)
Unit cell	$a = b = 88.48$ $c = 134.91$ $\alpha = \beta = 90°$ $\gamma = 120°$	$a = b = 88.61$ $c = 134.72$ $\alpha = \beta = 90°$ $\gamma = 120°$	$a = b = 88.50$ $c = 135.00$ $\alpha = \beta = 90°$ $\gamma = 120°$	$a = b = 88.42$ $c = 134.69$ $\alpha = \beta = 90°$ $\gamma = 120°$	$a = 95.11$ $b = 60.63$ $c = 74.98$ $\alpha = \beta = \gamma = 90°$
Temperature	100 K	120 K	120 K	120 K	100 K
Resolution (Å)	1.3	1.85	1.86	2.1	1.8
# Reflections	46,632	17,009	16,015	11,685	36,127
Completeness (%)	93.4(85)	96.2	92.53	94.3	88.3(89.6)
Redundancy	6.3(3.1)	8.2 (5.3)	4.3 (3.8)	7.5 (6)	4.1(4.5)
Rsym (%)	0.100 (0.857)	0.09 (0.85)	0.056 (0.575)	0.135 (0.958)	0.072 (0.655)
Average I/σ	18(2)	21 (2.7)	10 (2)	15 (2.8)	13(3)
R-factor/R-free (%)	20.0/22.7	17.4 (20.9)	18.3(22.4)	17.5(21.7)	21.4/26.8
Bond length (Å)	0.005	0.010	0.007	0.008	0.007
Bond angle (°)	1.06	1.19	1.03	1.06	1.15
# Protein atoms	1323	1338	1394	1323	3729
# Nucleotide atoms	32	32	32	32	96
# Magnesium ions	2	2	3	2	3
# Calcium ions	2	2	1	2	2
# Water molecules	184	164	110	119	238
# Acetate molecules	1	1	0	1	0